

Thermal plasma synthesis of SiC

Muralidharan Ramachandran · Ramana G. Reddy

Received: 6 July 2012 / Accepted: 12 October 2012 / Published online: 14 March 2013
© Shanghai University and Springer-Verlag Berlin Heidelberg 2013

Abstract Synthesis of silicon carbide has been carried out using thermal plasma processing technique using SiO_2 as the solid feed and CH_4 as the gaseous reducing agent. Thermochemical calculations have been performed varying the molar ratio of silicon dioxide and methane to determine the feasibility of the reaction. Experiments using a molar ratio of $\text{SiO}_2:\text{CH}_4$ equal to 1:2 produced maximum yield of SiC of about 65 mol % at a solid feed rate of 5 g/min. Mostly spherical morphology with some nanorods has been observed. The presence of Si had been observed and was quantified using XRD, HRTEM, Raman spectroscopy and X-ray photoelectron microscopy (XPS). Si acts as a nucleating agent for SiC nanorods to grow.

Keywords Silicon carbide · Thermal plasma · High resolution transmission electron microscopy (HRTEM) · Raman spectroscopy · X-ray photoelectron microscopy (XPS)

1 Introduction

Plasma is, in general, defined as the gas that is partially or fully ionized containing electrons, ions, neutral atoms and/or molecules. There can be two possible states of plasma, either thermal or non-thermal. Non-thermal plasmas are characterized by their low temperature while thermal plasmas have relatively very high temperatures and very high energy content. Partial thermal equilibrium is attained between the electrons and the heavy particles of the plasma

plume. In the mid to late twentieth century, thermal plasmas have been tested and used extensively in many applications such as extractive metallurgy, process metallurgy, plasma spray coatings, plasma welding and cutting, synthesis of advanced materials and toxic and hazardous waste treatment, just to name a few. Plasma spray coating was an \$800 million industry as reported in 1990 [1] and rose up to a \$1.35 billion in 1997 [2].

Synthesis of advanced materials has become one of the most important applications of thermal plasma due to its high temperature, high enthalpy, clean reaction environment, and use of inexpensive feed materials. High purity products are obtained as the reaction takes place in gaseous phase and products are obtained faster due to the enhanced reaction kinetics. Rapid quenching from very high temperatures creates a steep temperature gradient aiding the formation of fine sized particles. These fine particles can reach near-theoretical density on sintering which will also lead to improved mechanical properties. In spite of the numerous advantages of the thermal plasma processing technique, there are some inherent drawbacks, such as engineering and design difficulties, that can be overcome only with a detailed understanding of specific reaction mechanisms. High installation and power consumption costs, recycling costs of the process (off) gases from the plasma reactor are some of the other major concerns that need to be answered for an efficient operation of the process. The processes taking place inside the reactor and reaction mechanisms are also difficult to understand and are specific to the reactor system.

Literature is abundant on the types of plasma arcs and their uses and advantages in materials production [3–5]. Production of AlN [6], $\beta''\text{-Al}_2\text{O}_3$ and diamond [7] have been reported in the literature. Metallic and ceramic compounds such as magnesium, titanium carbide, and zinc

M. Ramachandran · R. G. Reddy (✉)
Department of Metallurgical and Materials Engineering,
The University of Alabama, Tuscaloosa, AL 35487, USA
e-mail: rreddy@eng.ua.edu

ferrite have been synthesized using this processing technique [3–12]. Several composite materials such as Fe-TiN, Fe-TiC, Fe(Ti)-TiC, Al(Ti)-TiC, and Al-SiC [13–15] have also been successfully synthesized. The use of thermal plasma for the production of fine and ultrafine powders has been patented by Celik et al [16]. The process variables such as plasma power, powder feed rate, and molar ratio of the reactants influence the product phases and their yield.

Silicon carbide is a material of interest due to its excellent properties. Some of the properties include high strength (tensile strength is equal to 160 MPa), hardness and elastic modulus (421 ± 10 GPa). This low density (3.165 g/cm^3) ceramic also possesses lower thermal expansion coefficient, excellent resistance to thermal shock and high thermal conductivity. It also has chemical inertness to numerous corrosive media. Such excellent properties of silicon carbide make it a good candidate for application in numerous fields. It is also a good semiconductor material with its conductivity dependant on the type and amount of dopant used.

Silicon carbide can be synthesized using one of the oldest methods known as Acheson method [17]. In this process silica, carbon, sawdust and common salt are mixed and heated in a resistive heating furnace at $2,700 \text{ }^\circ\text{C}$ [18]. After allowing reaction to occur, the temperature is decreased slowly. The final product of this process is mainly 6H-SiC. The yield of this process and reproducibility make it not a good candidate for commercial production of SiC.

Lely method [19] followed later by improved Lely method [20, 21] uses carbon crucible concentrically covered with a porous layer of SiC. The charge is loaded into the crucible and heated in a furnace to about $2,500 \text{ }^\circ\text{C}$. SiC platelets form on the inner side of the porous SiC layer. The predominant phase of SiC is still 6H-SiC similar to Acheson method. The lack of control over spontaneous nucleation and low yield are major drawbacks of the Lely and improved Lely processes. Hence, this process is also not commercially viable.

Seeded sublimation growth technique, also known as the modified Lely method [22], uses a seed, and source material in a graphite crucible at temperatures between $1,800$ and $2,600 \text{ }^\circ\text{C}$ in Ar atmosphere from 10^{-4} to $1 \times 10^5 \text{ Pa}$. In one configuration, the seed is at the bottom and the source material is on the top separated by a cylindrical graphite diaphragm [23]. Diffusion controls the kinetics of species transport and the difference in temperature between the seed and the source acts as a driving force, where the seed temperature is maintained slightly lower than the source temperature. In the second configuration [24], the seed is at the top and the source is at the bottom and there is no graphite diaphragm used. Due to the high yield of this process [25], it is used extensively today as a commercial production technique for SiC.

Sublimation sandwich method [26], chemical vapor deposition (CVD) [27], and liquid phase epitaxy (LPE) [23, 28] are some of the other techniques by which SiC can be synthesized. As SiC is also used as a semiconductor material, doping is usually done during the synthesis of the material. Al for *p*-type and $\text{N}_2/\text{Si}_3\text{N}_4$ for *n*-type are the most commonly used dopants. Vanadium doping is used to make semi-insulating SiC. SiC exists in three major polymorphs, 3C-SiC (also known as α -SiC), 4H-SiC and 6H-SiC (also known as β -SiC). β -SiC exists in hexagonal crystal structure while α -SiC is in cubic-zinc blende structure.

In the present work, thermal plasma synthesis technique was used to synthesize SiC using SiO_2 as the solid feed and CH_4 as the reducing gas. Experiments were conducted varying the molar ratio of the solid feed and the gaseous reducing agent. The plasma power and the rate of solid feed to the reactor were some of the other parameters that were studied. The product powders formed were then characterized for phase formation, morphology, and chemical binding energy.

2 Experiment

An in-house built plasma reactor was used in experiments for the synthesis of silicon carbide. The experimental setup of the plasma reactor system is shown in Fig. 1. It consists of a plasma power source that controls not only the current and the voltage to the plasma torch but also the gas pressure and the cooling water. The plasma gas used in the experiments was ultra high purity argon. The reducing and carrier gases, namely, methane and argon, pass through the powder feeder and enter the plasma reactor at the preset flow rate. The product powders are collected from the water-cooled quench coils in the quench chamber while the filter chamber retains any particulate matter from the exit flue gases.

Experiments were conducted using silicon dioxide, SiO_2 , (99.9 %, metals basis, Alfa-Aesar, MA, USA) as a powder feed to the plasma reactor. The plasma gas to the torch and the carrying gas to the powder feeder were ultra high purity Ar (AR UHP300 Gr 5.0, Airgas) and the reducing gas to the powder feeder was ultra high purity methane (ME UHP300 Gr 4.0, Airgas). The powder feeder was calibrated to obtain different solid feed rates, specifically 4 and 5 g/min of SiO_2 in the experiments. After the calibration of the powder feeder, the feed material was fed to the reactor which was set to the required power level and the product powders were collected.

The product powders obtained were characterized using X-ray diffraction (XRD), model Phillips X'Pert MPD, for phase analysis and the corresponding volume fractions of

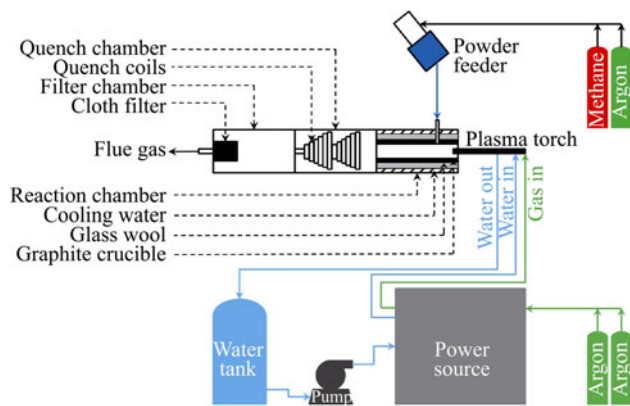


Fig. 1 Schematic of thermal plasma processing system

phases were calculated using direct comparison method. Scanning electron microscope (SEM), model JOEL 7,000 FE SEM, equipped with energy dispersive spectrometer (EDS) was used to determine the morphology of the product powders and determine the elemental composition. Transmission electron microscopy (TEM), model Tecnai F-20 TEM, was used to determine the morphology of the product powders. High resolution TEM (HRTEM) was used in observing the lattice fringes and subsequent calculation of d -spacing while scanning tunneling electron microscopy (STEM) was used to determine the phase contrast in material and determine the elemental composition. Raman spectra of product powders were obtained with a Bruker Senterra Raman microscope, using 785 nm wavelength, 1 mW laser source at a $50\times$ magnification. X-ray photoelectron spectroscopy (XPS), model KRATOS AXIS 165 XPS/Auger, was used to determine the chemical binding states of the product powders.

3 Results

3.1 Thermochemistry

Thermochemical calculations were done on the SiO_2 : CH_4 system varying the molar ratio of methane to SiO_2 from 0.8 to 5 using HSC Chemistry 5.1[®] [29]. The calculations are based on the principle of minimization of Gibb's energy [30] for a set of reactants at a given temperature and pressure. The equation describing this principle is given below:

$$G = \sum_{\text{gas}} n_i (g_i^0 + RT \ln P_i) + \sum_{\text{solution}} n_i (g_i^0 + RT \ln X_i + RT \ln \gamma_i) + \sum_{\text{pure condensed phase}} n_i g_i^0, \quad (1)$$

where G is the total Gibbs energy of the system, g_i^0 standard molar Gibbs energy of species i at temperature T and pressure P , n_i number of moles of species i , P_i the partial pressure of species i , X_i mole fraction of species i , and γ_i is the activity coefficient of species i .

The amount of theoretical product formation as a function of moles of methane in the feed at 1,520 °C is shown in Fig. 2. The equilibrium composition shows an increase in the amount of SiC with an increase in methane concentration in feed from 0.8 mol and reaches a maximum at 3 mol of methane. The theoretical yield at a methane molar ratio of 3 is about 98 mol %. The yield was calculated only based on the condensed phases formed and any gaseous products formed were omitted. The SiC formation decreases from 3 to 5 mol of methane with a corresponding increase in the amount of carbon as shown in Fig. 2. There was almost no SiO_2 presence at this temperature while small amounts of C and Si were observed. Similar calculations were done at other temperatures. At relatively lower temperatures, such as at 1,220 °C, SiO_2 reduced is relatively small. The amount of carbon at 1,220 °C increases with increase in the amount of methane consistent with the small amount of SiO_2 reduced. The amount of SiC formation is very less and is less than 1 mol % at all molar ratios of methane. When the temperature is increased to 2,120 °C, SiO_2 is converted to SiO in gaseous phase at lower molar ratios of methane. Silicon forms when molar ratio of methane is increased above 1 and its amount is a maximum at 2 mol of methane and is about 50 mol %. SiC forms only when the molar ratio of methane is 3 and its amount is about 63 mol %. The amount of C increases and SiO decreases with the increase

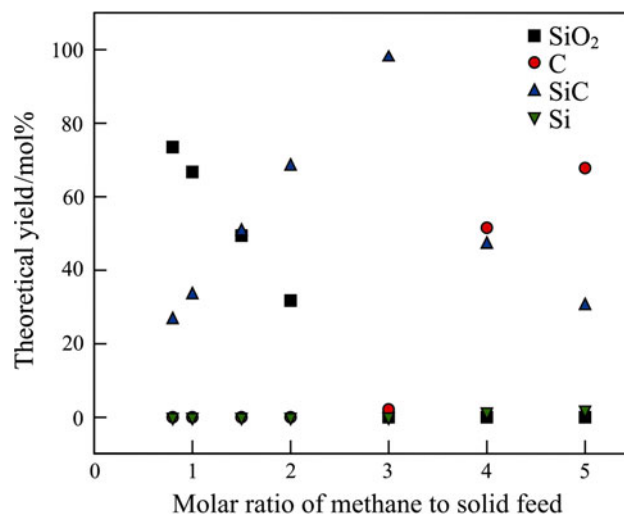


Fig. 2 Thermochemical calculations to determine stable phases as a function of amount of methane in feed at 1,520 °C

Table 1 Experimental conditions for the production of SiC using thermal plasma

Expt. #	Raw materials	Molar ratio	Plasma power/kW	Feed rate/(g·min ⁻¹)
1	SiO ₂ :CH ₄	1:1	21.6	5
2	SiO ₂ :CH ₄	1:0.8	21.6	5
3	SiO ₂ :CH ₄	1:1.5	21.6	5
4	SiO ₂ :CH ₄	1:1	18.9	5
5	SiO ₂ :CH ₄	1:2	21.6	5
6	SiO ₂ :CH ₄	1:2.5	21.6	5
7	SiO ₂ :CH ₄	1:1	21.6	4
8	SiO ₂ :CH ₄	1:2	21.6	4
9	SiO ₂ :CH ₄	1:3	21.6	4

in the amount of methane. At extremely high temperature, for example at 3,010 °C, there was no formation of SiC. SiO₂ is converted to SiO (g) similar to 2,120 °C at lower molar ratios of methane. Si forms above a molar ratio of methane greater than 1 with its yield a maximum at 2 and is about 58 mol %. The amount of SiO (g) decreases and the amount of C increases with the increase in the methane concentration.

It is concluded from thermochemical calculations that formation of SiC is favorable at lower molar ratios of methane and is a maximum at 3. Favorable temperatures for the formation of SiC are from about 1,500–2,100 °C. Formation of Si is favored at lower molar ratios of methane as well but is a maximum at 2 mol. Formation temperatures favorable for Si are from about 2,100–3,000 °C. Formation of carbon increases steadily with the increase of methane in the feed. Relatively very low amount of SiC is formed at very low (<1,500 °C) and at very high (>2,100 °C) temperatures. These observations led to the design of experiments with the variation in the mole ratio of methane to SiO₂ between 0.8 and 3, two different plasma powers 18.9 and 21.6 kW and two different solid feed rates, 4 and 5 g/min of SiO₂. The experimental conditions are given in Table 1.

3.2 Characterization of product powders

3.2.1 XRD

XRD was done on product powders from experiments to determine the product phases. The XRD patterns from experiments with varying molar ratios of CH₄ to SiO₂ from 0.8 to 2.5, a constant plasma power of 21.6 kW and a constant feed rate of 5 g/min are shown in Fig. 3. SiC is the major phase in all the experiments with the variation of molar ratio of methane to SiO₂. Formation of relatively higher quantities of Si was observed at lower molar ratios of methane. The amount of SiO₂ varies inconsistently with the variation in the molar ratio of methane. The amount of carbon in product powders increases with the increase in

the molar ratio of methane, but the relative amount does not exceed a maximum of 20 mol %.

Figure 4 shows the XRD patterns of the product powders from experiments with varying molar ratios of methane to SiO₂ from 1 to 3, a constant feed rate of 4 g/min and a constant power of 21.6 kW. SiC is the major phase in the experiments similar to that observed in the 5 g/min feed rate experiments. High amounts of silicon are observed only in the case of 1:1 ratio of SiO₂:CH₄ which decreases with the increase in the amount of methane. The relative amounts of SiO₂ and C in the product powders increase with an increase in the molar ratio of methane to 2 and 3.

3.2.2 Lattice constant and crystallite size

The unit cell lattice constant a was calculated for SiC in its cubic form synthesized at varying molar ratios of methane in the feed. Equation (2) described below was used in the calculation of lattice constant values:

$$\frac{1}{d^2} = \frac{h^2 + k^2 + l^2}{a^2}, \quad (2)$$

where d is the spacing between two consecutive ($h k l$) planes and a is the cubic unit cell lattice constant. The strongest diffraction peak for SiC, namely, the (1 1 1) peak was used in the calculations. The calculated lattice constant values were compared with that published in the standard PCPDF card (04-010-5699) ($a = 4.3588 \times 10^{-10}$ m).

Figure 5 shows the variation of the lattice constant as a function of one of the processing parameters, namely, the molar ratio of methane. The lattice parameter from the standard PCPDF data is shown in blue dashed line. As can be seen from the graph, the lattice constants values are way below the standard data for the molar ratios of methane varying from 0.8 to 2.0 with the exception of 1. The value of a for the experiment with methane molar ratio of 2.5 is way higher than the standard data. The plot also shows the crystallite size of the formed SiC as a function of the methane molar ratio. At very low molar ratios of methane

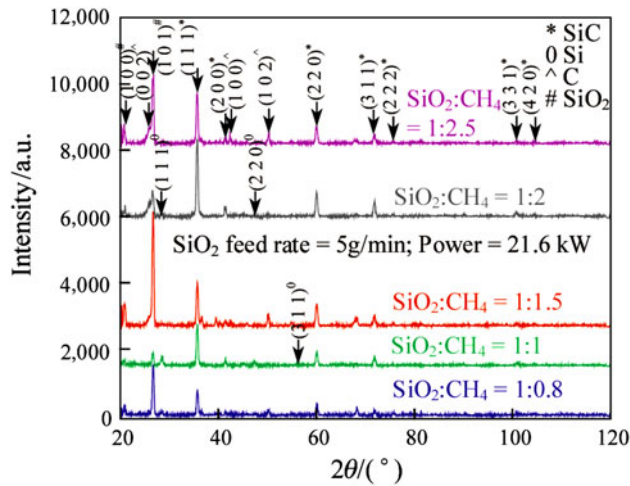


Fig. 3 XRD patterns of product powders formed at various amounts of methane in the feed and at a solid feed rate of 5 g/min SiO_2

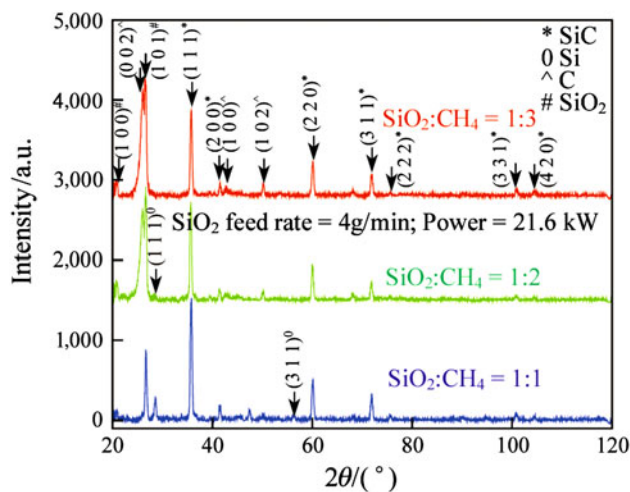


Fig. 4 XRD patterns of product powders formed at various amounts of methane in the feed and at a solid feed rate of 4 g/min SiO_2

the crystallite size is less than 10 nm. At higher molar ratios above 1, the crystallite size increases to over 20 nm in size.

It can be concluded that the lattice expansion or contraction is observed in the product powders obtained from thermal plasma synthesis. The closest match to the standard PCPDF data was obtained in the case of $\text{SiO}_2:\text{CH}_4$ equal to 1:1. It can also be concluded that lower molar ratios of methane, i.e., $\text{SiO}_2:\text{CH}_4 \leq 1:1$, yield relatively lower crystallite sizes compared to higher molar ratios of methane.

3.2.3 Volume fraction calculation

To determine volume fraction of product powders from the XRD patterns, direct comparison method was used. The volume fraction calculation was done on the product

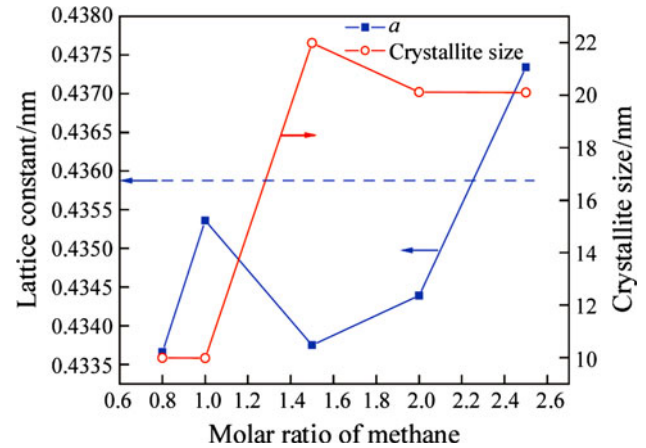


Fig. 5 Calculated lattice constant and observed crystallite size of synthesized SiC from XRD patterns

powders in condensed phase. Any products that escaped the reaction chamber in gaseous phases such as SiO are not accounted for. Similarly, amorphous phases that are present in the product powders will not show peaks in the XRD pattern. They will rather add to the background and hence, are not accounted for in these calculations. Equation (3) describes the expression for the calculation of volume fraction of product powders using direct comparison method. Some of the constants required to solve for the volume fraction were obtained from Cullity [31]. The atomic positions of the elements in unit cell were obtained from ICDD cards [32].

$$\frac{I_{\text{SiC}}}{I_{\text{SiO}_2}} = \frac{R_{\text{SiC}}c_{\text{SiC}}}{R_{\text{SiO}_2}c_{\text{SiO}_2}}, \quad \frac{I_{\text{Si}}}{I_{\text{SiO}_2}} = \frac{R_{\text{Si}}c_{\text{Si}}}{R_{\text{SiO}_2}c_{\text{SiO}_2}}, \quad (3)$$

$$\frac{I_{\text{C}}}{I_{\text{SiO}_2}} = \frac{R_{\text{C}}c_{\text{C}}}{R_{\text{SiO}_2}c_{\text{SiO}_2}}, \quad c_{\text{SiC}} + c_{\text{SiO}_2} + c_{\text{Si}} + c_{\text{C}} = 1,$$

where I_{SiC} , I_{SiO_2} , I_{Si} and I_{C} represent the intensities of SiC, SiO_2 , Si and C respectively; c_{SiC} , c_{SiO_2} , c_{Si} and c_{C} represent the volume fractions of SiC, SiO_2 , Si and C respectively; and R_{SiC} , R_{SiO_2} , R_{Si} and R_{C} represent the volumes of inverse unit cell lattices of SiC, SiO_2 , Si and C respectively.

The volume fraction calculated using the direct comparison method was converted to corresponding mole percent values using molecular weights and densities of corresponding pure condensed phases.

3.2.4 XPS

XPS spectra of product powders from experiment 1 were obtained to determine the chemical binding states of species. Figure 6 shows the Si 2p binding energy of powders from experiment 1. The original peak was de-convoluted into three individual peaks. The peak at a binding energy of about 101.6 eV corresponds to elemental Si bonding, while

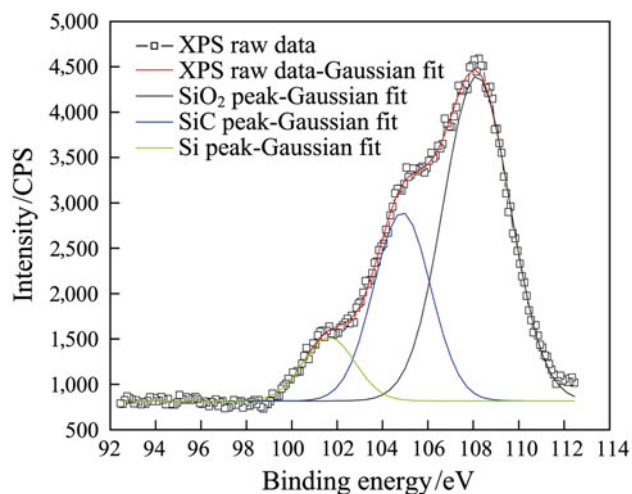


Fig. 6 XPS of product powders from experiment 1 showing the Si 2p peak resolved into SiO₂, SiC and Si peaks

the peak at about 104.8 eV corresponds to the SiC bonding. The peak at about 108 eV corresponds to SiO₂ in the product powders. The peak positions for SiO₂ and SiC have also been reported in the literature [33, 34]. The change in the peak positions by 2–4 eV might be due to the fluorescence effect of the powders used to determine the binding energy. This provides further substantiation for the presence of Si, SiC and SiO₂ in the product powders.

3.2.5 SEM

SEM was used to determine the morphology of the product powders from the experiments. Figure 7a and b shows the morphology of the products from experiment 1 with methane molar ratio of 1, solid feed rate of 5 g/min and a power of 21.6 kW. The particles are almost spherical with an average diameter varying between 200 and 500 nm as seen from Fig. 7a at low magnification. It can also be seen from Fig. 7b (high magnification) that formation of nanorods is observed in the morphology.

The product powder's morphology from experiment 2 with methane molar ratio of 0.8, solid feed rate of 5 g/min and a power of 21.6 kW is shown in Fig. 8. It is seen that the nanorod formation is prominent from this experiment as well. Figure 9, on the other hand, shows the morphology of powders from experiment 5 with 2 mol of methane and 5 g/min solid feed. Mostly spherical particulates are observed in this case with an average particle size distribution between 200 and 500 nm.

Morphology of product powders from experiment 7 using lower solid feed rate of 4 g/min SiO₂, power of 21.6 kW and a methane molar ratio of 1 is shown in Fig. 10. Similar to the higher feed rate counterpart (see

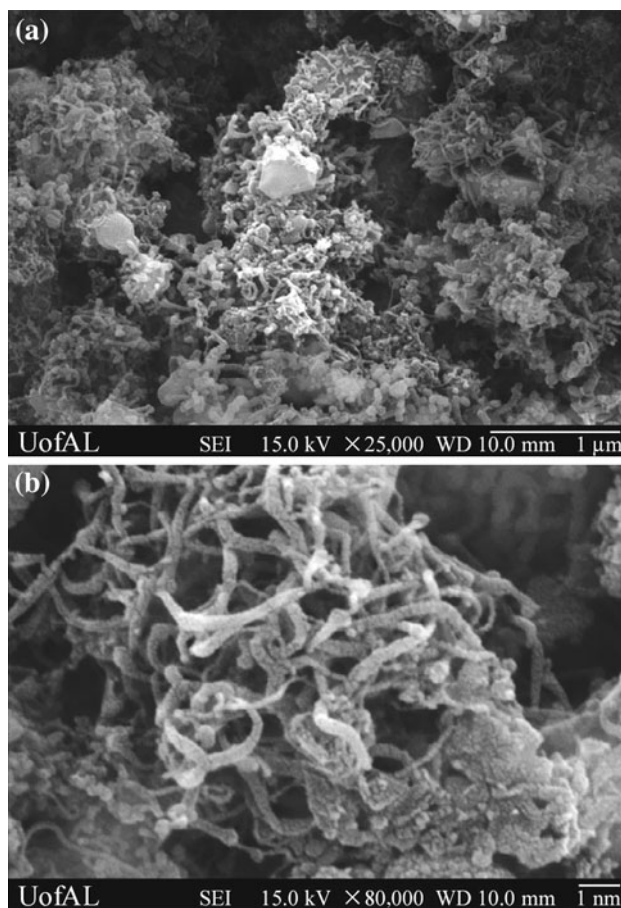


Fig. 7 SEM images showing the morphology of product powders from experiment 1 at **a** low and **b** high magnifications

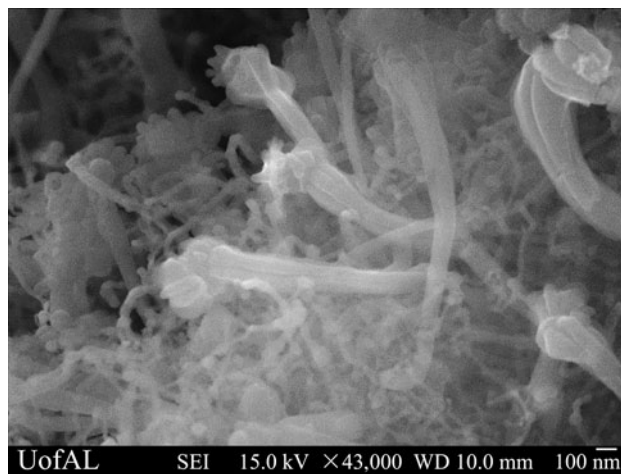


Fig. 8 SEM image showing the morphology of product powders from experiment 2

Fig. 7), the product powders consist of particulate matter no bigger than 500 nm. Along with the particles, nanorod formation is also evident from the micrograph.

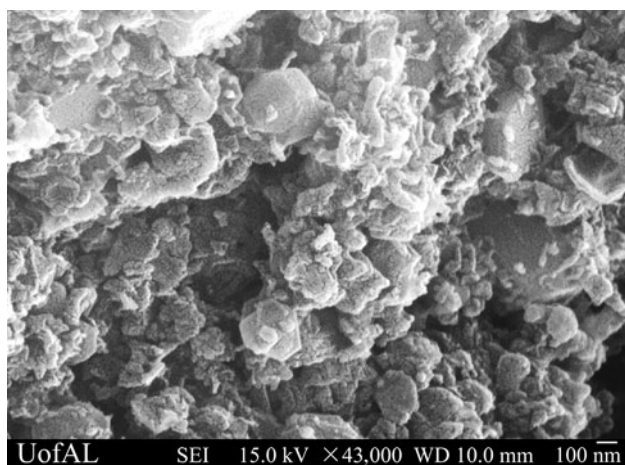


Fig. 9 SEM image showing the morphology of product powders from experiment 5

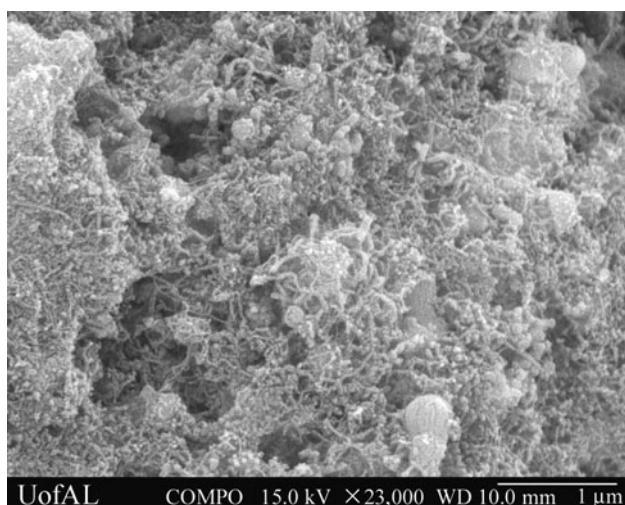


Fig. 10 SEM images showing the morphology of product powders from experiment 7

3.2.6 TEM

The morphology of the product powders were further analyzed at high resolution using TEM. The powders from experiment 1 using 5 g/min solid feed rate, 21.6 kW power and methane molar ratio of 1 is shown in Fig. 11. The nanorods shown in Fig. 11a are about 20–50 nm in diameter. This is similar to that observed in the SEMs. High resolution TEM image was obtained from the product powders of experiment 1, as shown in Fig. 11b. The d -spacing calculations show the presence of SiO_2 in the sample. The d -spacing of about 0.33 nm corresponds to the (1 0 1) plane of SiO_2 .

STEM image of product powders from experiment 1 is shown in Fig. 12a. The image shows darker spot that consists of numerous nanoscale particles. The darker

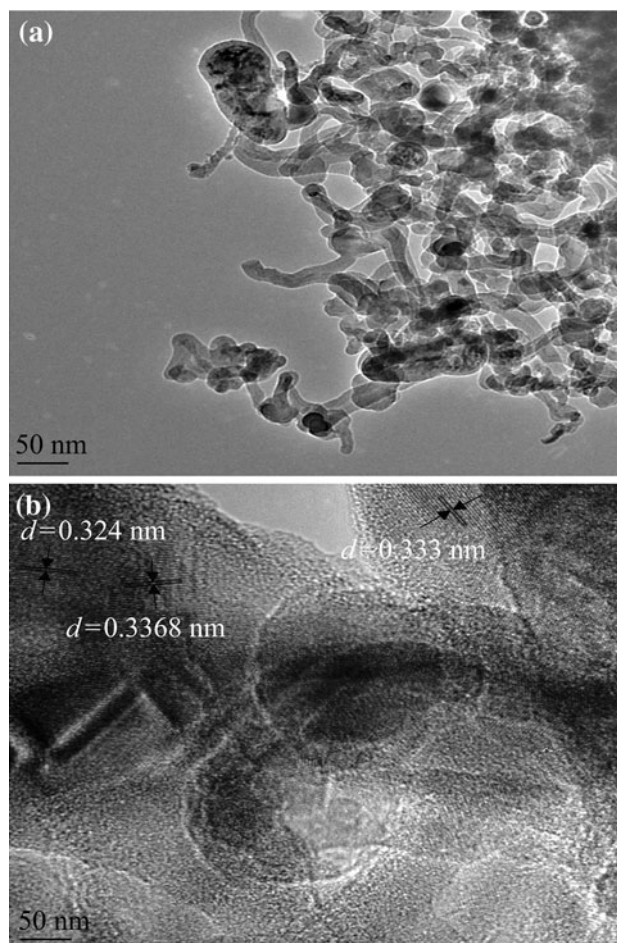


Fig. 11 TEM images showing the morphology of the product powders from experiment 1

spheres correspond to Si while the lighter areas surrounding it correspond to SiO_2 . Figure 12b shows an EDS spectra of the spot 1 marked in red on the STEM image. It is observed that Si is the major component, with a small quantity of elemental O observed due to the surrounding SiO_2 . Cu in the EDS is from the copper grid used to load the powder sample.

Experiment 2 shows the presence of nanorods as shown in Fig. 13a similar to that observed from experiment 1 (see Fig. 11a). The nanorods formed from experiment 2 were about 20–50 nm in diameter. High resolution image of the product powders shows the presence of Si (see Fig. 13b). The d -spacing calculation on the lattice fringes show that the d -spacing of about 0.31 nm corresponds to the close-packed (1 1 1) plane of Si. The tip of a nanorod shown in Fig. 13b is Si.

SiO_2 is also found in the product powders from experiment 2 as suggested by the d -spacing of about 0.33 nm. Figure 14 shows SiO_2 as a single crystal. The insets show a magnified portion from the high resolution image and the corresponding diffraction pattern of the area. The width of

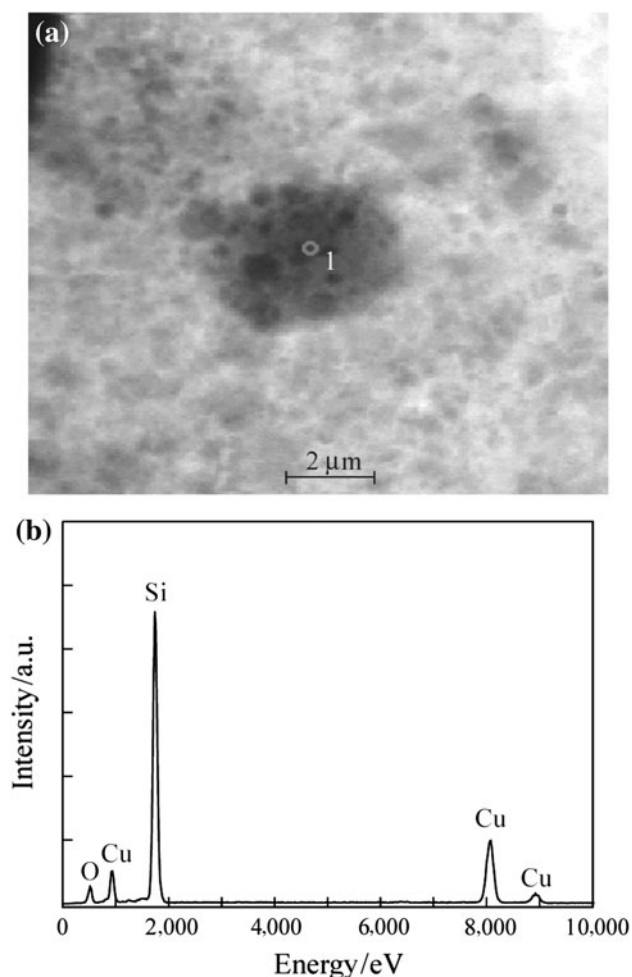


Fig. 12 a STEM images of product powders from experiment 1 and b EDS corresponding to spot 1

the nanoparticle shown in the micrograph is less than 20 nm in size. This suggests one of the two following phenomena taking place inside the reactor. First, the silicon dioxide solid feed completely vaporized and recrystallized into smaller particles due to shorter residence time. Second, complete vaporization did not occur while surface melting and drastic particle size reduction took place inside the plasma reactor.

3.2.7 Raman spectra

Inelastic Raman spectra measurements were made on product powders from experiments 1, 2 and 3, as shown in Fig. 15. Presence of carbon in all the samples is substantiated by the peaks at wavenumbers 1,302.17, 1,573.89 and 2,593.51 cm^{-1} . The peaks at wavenumbers 789 and 925.63 cm^{-1} correspond to SiC. It is reported in the literature that these wavenumbers correspond to SiC in nanorod form [35]. The peaks corresponding to SiC are observed only in experiments 1 and 2 but in experiment 3. Same is

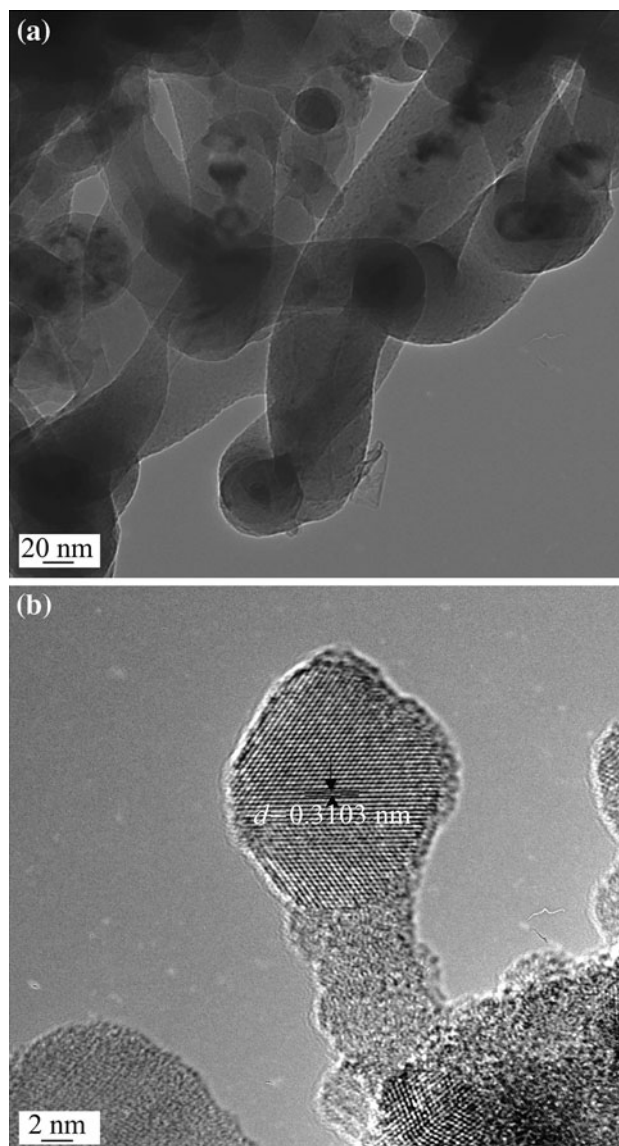


Fig. 13 TEM images showing the morphology of the product powders from experiments 2

the case with the peaks corresponding to Si at wavenumber 512.49 cm^{-1} . Noticeable amounts of Si and SiC nanorods are present in the product powders from experiments 1 and 2, similar to the volume fraction calculation using XRD.

4 Discussion

4.1 Effect of molar ratio of methane

The effect of molar ratio of methane for experiments with constant power of 21.6 kW and 5 g/min solid feed rate is shown in Fig. 16. As can be seen, SiC is the major phase formed with a minimum of about 40 mol % and a

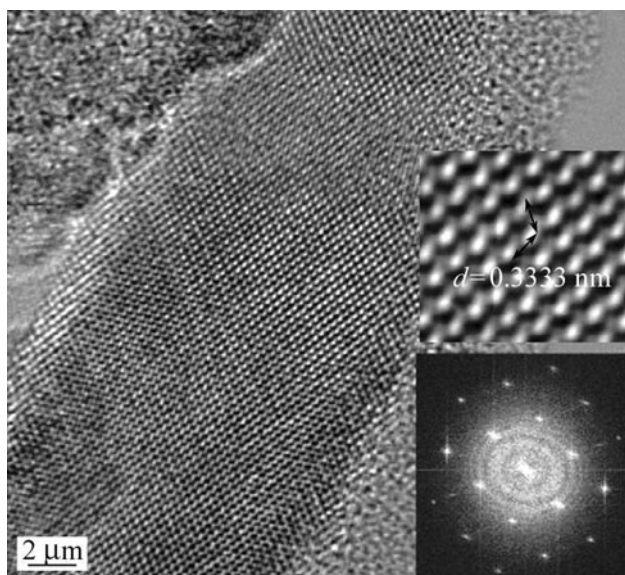


Fig. 14 TEM image showing a single crystal SiO_2 from experiment 2 (magnified image (top inset) and diffraction pattern (bottom inset))

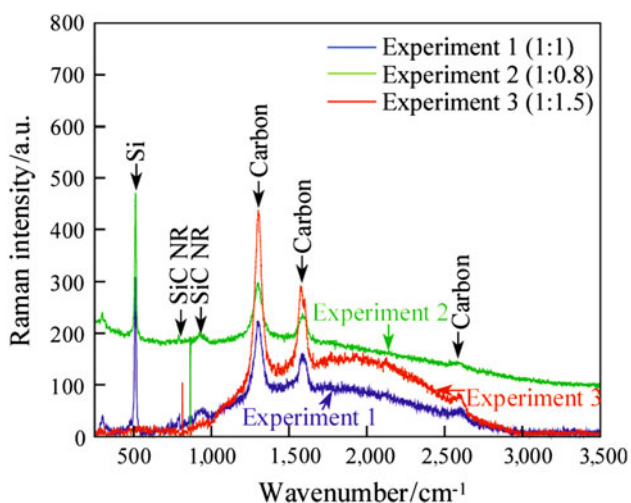


Fig. 15 Raman spectra of product powders from experiments 1, 2 and 3 using a solid feed rate of 5 g/min

maximum of about 65 mol % at 2 mol of methane in the feed. The amount of Si is a maximum at 1 mol methane and is determined to be about 40 mol %. SiO_2 in the product powder varies between a minimum of about 5 mol % and a maximum of about 35 mol %. The amount of C is relatively low in the experiments using a feed rate of 5 g/min of SiO_2 and is a maximum of about 20 mol % at a methane molar ratio of 2.5.

Similar calculations were done on the product powders from experiments conducted at a solid feed rate of 4 g/min of SiO_2 and a constant power of 21.6 kW. It can be seen

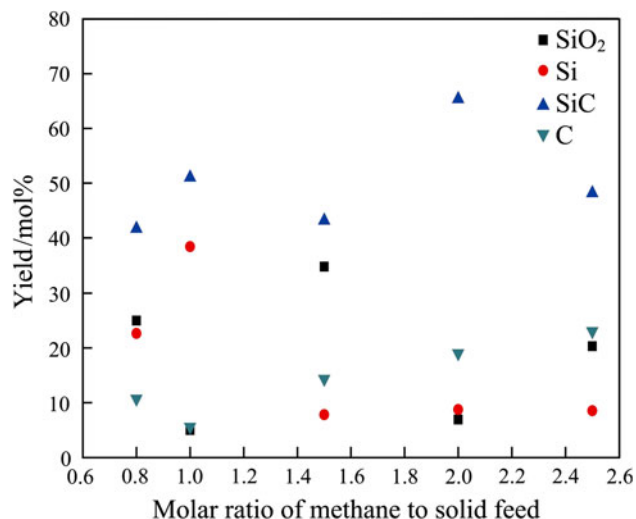


Fig. 16 Effect of molar ratio of methane at a solid feed rate of 5 g/min SiO_2 and plasma power of 21.6 kW

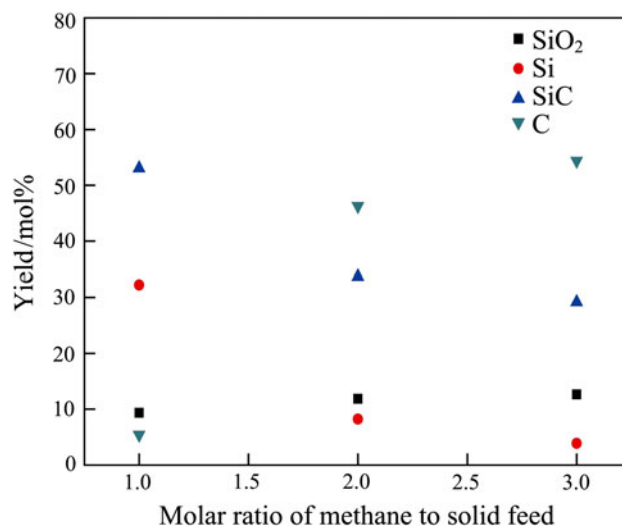


Fig. 17 Effect of molar ratio of methane at a solid feed rate of 4 g/min SiO_2 and plasma power of 21.6 kW

from Fig. 17 that the amounts of SiC and Si are both a maximum at a methane molar ratio of 1. The experimental yields of SiC and Si were found to be about 55 and 35 mol % respectively. The amount of SiO_2 in the product powders seems to be almost constant with the change in the moles of methane and is about 10 mol %. An enormous increase in the amount of C was observed with the increase in the molar ratio of methane to 2 and 3. While the C concentration was about 5 mol % at a methane molar ratio of 1, it increased to 45 and 55 mol % with increase in moles of methane to 2 and 3 respectively.

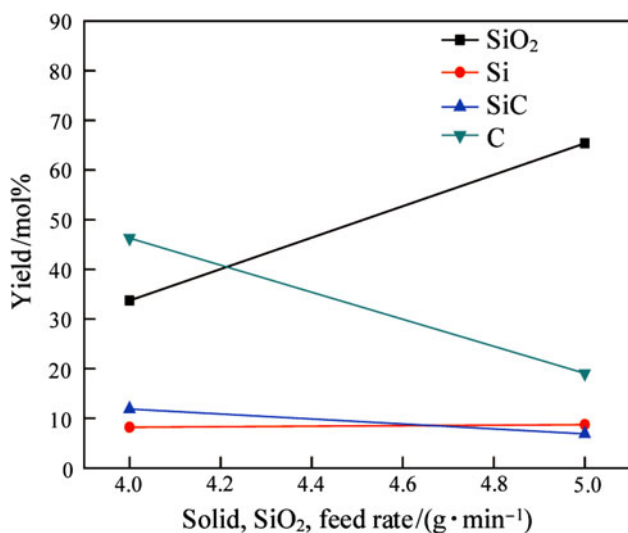


Fig. 18 Effect of solid, SiO₂, feed rate at a molar ratio of SiO₂:CH₄ equal to 1:2 and a plasma power of 21.6 kW

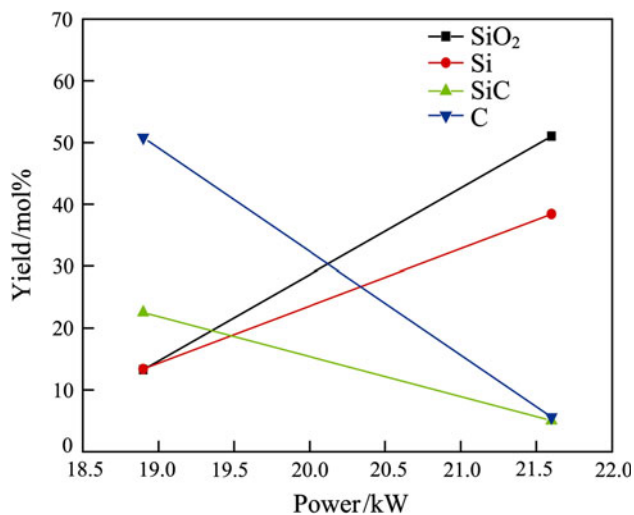


Fig. 19 Effect of plasma power on the yield of products at a solid feed rate of 5 g/min and a molar ratio of SiO₂:CH₄ equal to 1:1

4.2 Effect of solid feed rate

The effect of solid, SiO₂, feed rate on the experimental yield of product powders were compared at two different molar ratios of methane, 1 and 2. At lower molar ratio of methane equal to 1, the effect of the solid feed rate is almost negligible. The maximum relative variation in product yield is (± 16) mol %. This is, of course, not the case at a molar ratio of 2.

The effect of solid feed rate at a molar ratio of SiO₂:CH₄ equal to 1:2 is shown in Fig. 18. The increase in the yield of SiC is almost double when the feed rate increases from 4 to 5 g/min. The relative amounts of SiO₂ and carbon have

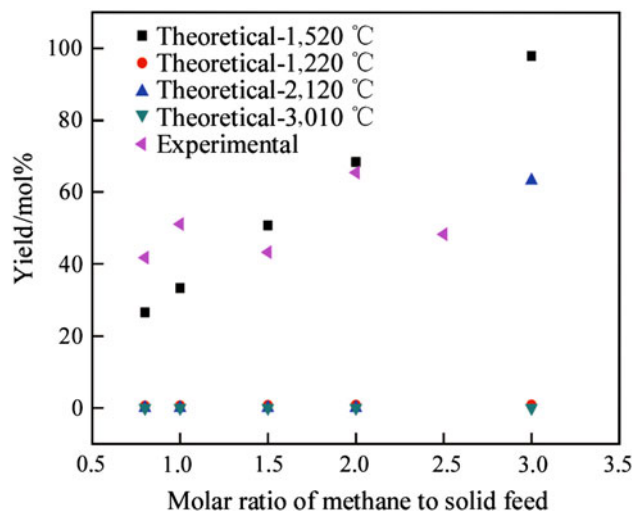


Fig. 20 Comparison of theoretical yield of SiC at various temperatures to experimental yield of product powders formed at various amounts of methane in feed and a solid feed rate of 5 g/min

reduced in half while the yield of Si remains unaltered with the increase in the feed rate.

4.3 Effect of plasma power

The effect of plasma power was studied at a constant solid feed rate of 5 g/min and constant molar ratio of SiO₂:CH₄ equal to 1:1. The two plasma powers used were 18.9 and 21.6 kW. The effect of increase in the plasma power is shown in Fig. 19.

An increase in power from 18.9 to 21.6 kW increased SiC yield by 4 times. The experimental yield of Si also increased by 3 times compared to the yield at lower power. The increase in power also resulted in corresponding decrease in the amount of SiO₂ by 4 times and a drastic decrease in the amount of carbon by almost 10 times.

4.4 Comparison of theoretical and experimental yield

Temperature is one of the implicit parameters that are varied with the change in the plasma power. Hence the experimental yield of SiC at various molar ratios of methane using 5 g/min feed rate and 21.6 kW plasma power was compared with theoretical yield of SiC at various temperatures.

Figure 20 shows the comparison of the theoretical yield and the experimental yield of SiC. It is observed from the graph that the yield of SiC at lower molar ratios of methane follows theoretical yield at 1,520 °C and maximum variation is about 15 mol %. The variation in yield is lower at molar ratios of 1.5 and 2 mol of methane per mole of SiO₂ at 1,520 °C. The maximum variation is seen about 30 mol % at a methane molar ratio of 2.5. In spite of the

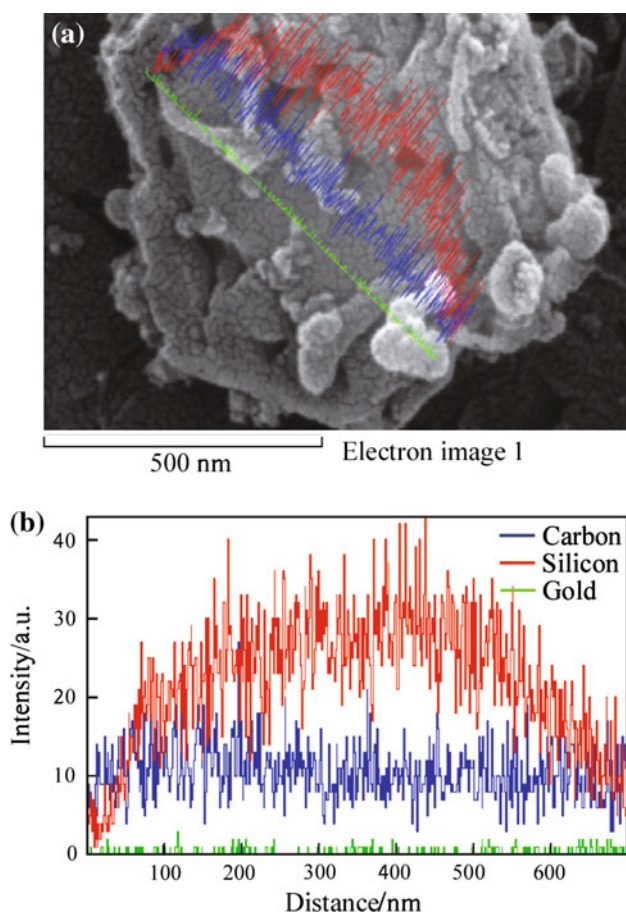


Fig. 21 Line profile elemental analysis of product powder from experiment 1

small variation in the comparison of yield, it can be concluded that the formation temperature of SiC inside the plasma reactor is in the range of 1,500–2,100 °C and is closer to 1,500 °C for the given experimental conditions of 5 g/min SiO₂ feed rate and 21.6 kW plasma power.

4.5 SEM-EDS

A single particle of about 700 nm in width from experiment 1 (power–21.6 kW; SiO₂:CH₄ is equal to 1:1; solid feed rate is equal to 5 g/min) was analyzed using EDS and an elemental line profile was generated as shown in Fig. 21a. It is confirmed from the elemental composition graph shown in Fig. 21b that the hexagonal particle is Si. The presence of carbon could be due to any SiC on the surface of the particle and also from the carbon tape used to load the sample. Gold is from the coating used to make the material electronically conductive so as to reduce the effect of charging and obtain good resolution.

A single nanorod of about 20–25 nm in diameter from experiment 1 was analyzed using EDS as shown in

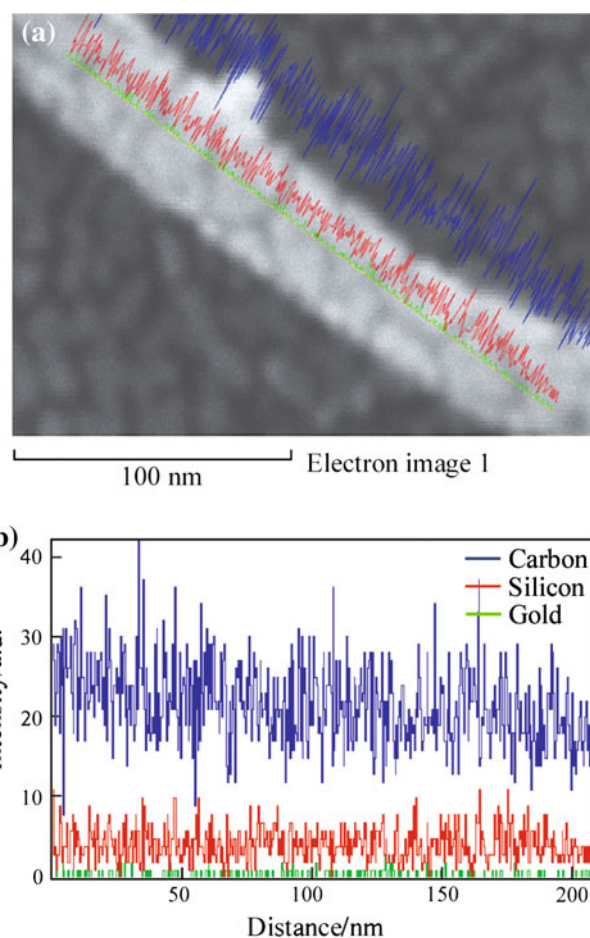


Fig. 22 Line profile elemental analysis of a SiC nanorod from experiment 1

Fig. 22a with its corresponding elemental line profile. The nanorod formed is SiC due to the presence of Si and C from the elemental analysis (see Fig. 22b). The presence of excess C is due to the carbon tape used to load the sample. As mentioned earlier, the gold is from the coating of the sample to make it conductive.

4.6 Formation of nanorods

It was also observed that the formation of nanorods was observed only when the molar ratio of methane in the feed was 1 or less. Correlating with the phases formed from the XRD patterns, it can be concluded that the formation of nanorods is due to the presence of Si in the product powders. This conclusion is justified by the presence of silicon at the tip of the nanorod (see Fig. 18b). Inelastic Raman spectra also show presence of high quantities of Si from experiments 1 and 2 and the corresponding formation of SiC nanorods, further justifying the formation of nanorods due to the presence of Si.

5 Conclusions

SiC was successfully produced using thermal plasma using SiO₂ as the solid feed and methane as the reducing gas. Thermochemical calculations suggest that the yield of SiC is a maximum at a temperature of 1,520 °C and a molar ratio of SiO₂:CH₄ equal to 1:3. Formation of Si and SiO (g) was also observed from the calculations. Experiments using a molar ratio of SiO₂:CH₄ equal to 1:2 produced the maximum yield of SiC with a solid feed rate of 5 g/min and a power of 21.6 kW. The unit cell lattice constant calculations show that lattice contraction or expansion occurs in the product powders during thermal plasma synthesis. Smaller crystallite sizes (100 nm) were observed at lower molar ratios of methane (≤ 1). Comparison between the theoretical and the experimental yield suggests that the temperature in the plasma reactor might be in the range of 1,500–2,100 °C. The size and shape of the final products changed with the change in the process parameters. Spherical particulate matter of no greater than 500 nm and nanorods of about 20–30 nm in diameter were observed. It was concluded from HRTEM, SEM-EDS and Raman analysis that Si acts as a nucleating agent for the nanorods to grow. XPS confirms the presence of Si, SiO₂ and SiC in the samples.

Acknowledgments Authors are pleased to acknowledge the financial support provided by ACIPCO, and the University of Alabama for this research work.

References

- Apelian D (1992) Materials synthesis: A new horizon for plasma processing. In: International symposium on thermal plasma applications in materials and metallurgical Processing, San Diego, USA, 1–5 Mar 1992
- Kassabji F, Jacq G, Durand JP (1998) Thermal spray application for the next millennium: A business development perspective. In: Proceedings of the 15th international thermal spray conference, Nice, France, 25–29 May 1998
- Taylor PR, Pirzada SA (1994) Thermal plasma processing of materials: a review. *Adv Perform Mater* 1:35–56
- Boulos MI (1991) Thermal plasma processing. *IEEE Trans Plasma Sci* 19(6):1078–1089
- Pfender E (1999) Thermal plasma technology: where do we stand and where are we going? *Plasma Chem Plasma Process* 19(1):1–31
- Oh SM, Park DW (1998) Preparation of AlN fine powder by thermal plasma processing. *Thin Solid Films* 316:189–194
- Fukumasa O, Sakiyama S (2000) Thermal plasma processing-synthesis of diamond and β -alumina. *Surf Coat Technol* 131:493–499
- White SW, Reddy RG (1999) Waste processing of MgO bag house dust using plasma arc technology. In: Mishra B (ed) *EPD Congress 1999*. TMS, Nashville, pp 687–697
- Reddy RG, Antony LVM (2003) The thermal plasma processing of fine powders. *J Manag* 55(3):19–22
- Reddy RG, Antony LVM (2003) Processing of SiC nano powders using thermal plasma technique. In: Proceedings of the international conference on nanotechnology: scientific challenges and commercial opportunities, Rhode Island, 17–18 Sep 2003
- Mohai I, Szépvölgyi J, Bertóti I et al (2001) Thermal plasma synthesis of zinc ferrite nanopowders. *Solid State Ionics* 141(142):163–168
- Tong L, Reddy RG (2005) Synthesis of titanium carbide nanopowders by thermal plasma. *Scripta Mater* 52:1253–1258
- Niyomwas S, Wu B, Reddy RG (2000) Synthesis and modeling of Fe–TiN composites by thermal plasma processing. In: Suryanarayana C, Thadhani NN et al (eds) *Ultrafine grained materials*. TMS, Nashville, pp 89–98
- Antony LVM (2004) Thermal plasma processing of Al–SiC ultrafine composites. Dissertation, The University of Alabama
- Tong L, Reddy RG (2006) In situ synthesis of TiC–Al(Ti) nanocomposite powders by thermal plasma technology. *Metall Mater Trans B* 37B:531–539
- US Patent 6,379,419 B1, 30 April 2002
- Acheson AG (1892) British Patent 17:911
- Knippenberg WF (1966) Growth phenomena in silicon carbide: preparative procedures. *Philips Res Rep* 18:170–179
- Lely JA (1955) Darstellung von einkristallen von siliziumcarbide und beherrschung von art und menge der eingebauten verunreinigungen. *Ber Deutsche Keramik Gesellschaft* 32:229–231
- Hamilton DR (1960) The growth of silicon carbide by sublimation. In: Connor JR, Smilestons J (eds) *Silicon carbide: a high temperature semiconductor*. Pergamon, Oxford, pp 45–51
- Novikov VP, Ionov VI (1968) Production of monocrystals of alpha-silicon carbide. *Growth Cryst* 6:9–21
- Tairov YM, Tsvetkov VF (1978) Investigation of growth processes of ingots of silicon carbide single crystals. *J Cryst Growth* 43:209–212
- Ziegler G, Lanig P, Theis D et al (1983) Single crystal growth of SiC substrate material for blue light emitting diodes. *IEEE Trans Electron Devices* 30(4):277–281
- Glass RC, Henshall D, Tsvetkov VF et al (1997) SiC-seeded crystal. *MRS Bull* 22(3):30–35
- Tairov YM (1995) Growth of bulk SiC. *Mater Sci Eng B* 29:83–89
- Karpov SY, Makarov YN, Mokhov EN et al (1997) Analysis of silicon carbide growth by sublimation sandwich method. *J Cryst Growth* 173:408–416
- Matsunami H, Kimoto T (1997) Step controlled epitaxial growth of SiC: high quality homoepitaxy. *Mater Sci Eng B* 20:125–166
- Epelbaum BM, Hofmann D, Muller M et al (2000) Top-seeded solution growth of bulk SiC: search for the fast growth regimes. *Mater Sci Forum* 338(342):107–110
- Roine A (2002) *HSC Chemistry Ver. 5.1*, Copyright© Outokumpu Research Oy, Pori, Finland
- Gokcen NA, Reddy RG (1966) *Thermodynamics*, 2nd edn. Plenum Publications, New York, pp 203–243
- Cullity BD (1978) *Elements of X-ray diffraction*, 2nd edn. Addison-Wesley, Reading
- Powder Diffraction File-4 (PDF-4)* (2011) International Centre for Diffraction Data (ICDD), Joint committee on powder diffraction Standards (JCPDS)
- Ryu Y, Tak Y, Yong K (2005) Direct growth of core-shell SiC–SiO₂ nanowires and field emission characteristics. *Nanotechnology* 16:S370–S374
- Galuska AA, Uht JC, Marquez N (1988) Reactive and nonreactive ion mixing of Ti films on carbon substrates. *J Vac Sci Technol A* 6(1):110–122
- Zhang SL, Zhub BF, Huanga F et al (1999) Effect of defects on optional phonon Raman spectra in SiC nanorods. *Solid State Commun* 111(11):647–651